IFUSP/P-38

AN ANALYSIS OF ELECTRODISINTEGRATION OF NUCLEI USING E1 VIRTUAL RADIATION SPECTRA EVALUATED WITH COULOMB DISTORTED WAVES

E.Wolynec, G.Moscati, O.D.Gonçalves*
and M.N.Martins*

Instituto de Física
Universidade de São Paulo
BRASIL

*Scholarship by Fundação de Amparo à Pesquisa do Estado de São Paulo - FAPESP.

ABSTRACT

Data on the ratio of photo to electrodisintegration of several nuclei (^{12}C, ^{63}Cu, ^{64}Zn, ^{109}Ag, ^{181}Ta and ^{197}Au) are compared with the theoretical ratios predicted by plane and distorted waves calculations. The analysis with distorted waves shows that all data are compatible with photoabsorption through dominant E1 transitions, as can be explained by the electric dipole sum rule. This outcome does not agree with published conclusions for high Z using plane waves approximation.

SUMÁRIO

Dados experimentais da razão entre foto e eletrodesintegração de vários núcleos (^{12}C, ^{63}Cu, ^{64}Zn, ^{109}Ag, ^{181}Ta e ^{197}Au), são comparados com resultados de cálculos efetuados utilizando - aproximação de ondas planas e de ondas distorcidas. Da análise- com ondas distorcidas resulta que todos os dados experimentais - são compatíveis com a hipótese de que a fotoabsorção processa-se dominantemente através de transições E1, o que pode ser explicado pela Regra de Soma para transições de dipôlo elétrico. Este resultado, para núcleos de Z alto, está em desacôrdo com conclusões baseadas na aproximação de onda plana, encontradas na literatura.

I - INTRODUCTION

The electroexcitation of nuclei is closely related to the corresponding process of photoexcitation. In both cases the nucleus receives its excitation energy through the interaction of an electromagnetic field with nuclear charges and currents. Indeed, in the theoretical calculations of the cross-sections, the matrix element involving the nuclear wave functions is the same. Performing the ratio of the two cross-sections, the unknown matrix element cancels out and a virtual photon spectrum can be defined, which gives the number of photons of average energy w, in the energy interval $w \pm \frac{dw}{2}$ [1].

$$N^{(\lambda L)}(E_1, w)\ \frac{dw}{w} = \frac{\sigma_e^{\lambda}(L, E_1, w)}{\sigma_\gamma^{\lambda}(L, w)} \qquad (1)$$

where

λ = label either E or M for electric or magnetic transitions;

L = multipole order

σ_e = cross-section for electron-nucleus excitation (integrated over all scattering angles);

σ_γ = cross-section for photon-nucleus excitation;

w = photon energy (either real or virtual);

E_1 = incident electron total energy.

Calculations of $N^{(\lambda L)}(E_1,\omega)$, considering a point nucleus and the incoming electrons as plane waves, PW, were carried out by Thie et al.[1], for E1, E2 and M1 multipolarities. The expression for E1 is:

$$N^{E1}_{PW}(E_1,\omega) = (\alpha/\pi)\left\{\left[(E_1^2 + E_2^2)/(E_1^2 - m_e^2)\right] \log\left[(E_1E_2+(E_1^2- - m_e^2)^{1/2} \times (E_2^2 - m_e^2)^{1/2} - m_e^2)/m_e\omega\right] - 2\left[(E_2^2 - m_e^2)/(E_1^2 - - m_e^2)\right]^{1/2}\right\} \qquad (2)$$

where:

$E_2 = E_1 - \omega$

m_e = electron's rest energy

α = fine structure constant

More recently, Gargaro and Onley[2] obtained computable expressions for $N^{(\lambda L)}$, for all multipole orders, using a distorted wave treatment, DW, Dirac-Coulomb wave functions for the basis states of the electron, assuming the electron is moving in the field of a point charge. The expression for $N^{(\lambda L)}$ is:

$$N^{(\lambda L)}_{DW}(E_1,\omega) = \left[(\alpha/\pi)(p_1/p_2)(E_1+m_e)(E_2+m_e)\omega^4(2L+1)^{-1}\right]\sum_{\kappa_1\,\kappa_2} S(\lambda) \times (2j_1+1)(2j_2+1) \times \left|C(j_1,j_2,L;\ \frac{-1}{2},\ \frac{1}{2})\ R^{(\lambda)}(\kappa_1,L,\kappa_2)\right|^2 \qquad (3)$$

where:

$p_1(p_2)$ = initial (final) electron momentum;

$S(\lambda)$ = projection operator which retains only those terms satisfying the selection rules for electric or magnetic transitions of multipole order L;

$R^{(\lambda)}$ = and remaining parameters are defined in ref. [2].

From Eq.(1), the total inelastic electron scattering cross-section may be expressed in a form similar to the - yield in photoexcitation experiments:

$$\sigma_e(E_1) = \int_0^{E_1-m_e} \frac{dw}{w} \sum_{\lambda L} \sigma_\gamma^\lambda (L,w) N^{(\lambda L)}(E_1,w) \quad (4)$$

Thus, expression (4) enables one to evaluate the electro-excitation cross-section, from the photoexcitation cross-section $\sigma_\gamma^\lambda(L,w)$. However $\sigma_\gamma^\lambda(L,w)$ is not an available experimental quantity. The measurements give $\sigma_\gamma(w) = \sum_{\lambda L} \sigma_\gamma^\lambda(L,w)$.

A number of experiments [3-7] comparing electro and photodisintegration of nuclei have been made with the aim of testing the multipolarity of transitions responsible for the photonuclear giant resonance. These experiments were carried out before the distorted wave treatment of virtual photon spectra [2] was available. Thus, the inability to fit expression (4) assuming E1 transition for the photodisintegration cross-section, as suggested by the sum rule, led to the assumption of the possible importance of E2 tran

sition. With this assumption the measured cross-sections were expressed as:

$$\sigma_\gamma(w) = \alpha\sigma_\gamma^E(1,w) + \beta\sigma_\gamma^E(2,w) \qquad (5)$$

where, α and β were constants determined by fitting expression (4) with the measured data. This procedure with α and β constants, involves the assumption that the cross-sections for E1 and E2 transitions have the same structure and differ only in magnitude. The use of plane waves led, for high Z, to β values of the same order or even higher than α, in desagreement with the generally accepted[8] E1 character of the giant resonance. For this reason we decided to reanalyse these data, using the distorted wave virtual photon spectra and assuming that the measured σ_γ for the giant resonance is predominantly E1:

$$\sigma_\gamma(w) = \sigma_\gamma^{E1}(w) \qquad (6)$$

that is, $\alpha = 1$ and $\beta = 0$ in (4).

II- EXPERIMENTAL DATA WITH THEIR ORIGINAL ANALYSIS

All experimental data analysed here consists of measured yields of radioactivities, $Y_e(E_1)$ and $Y_{br}(E_1)$, produced, respectively, when electrons of total energy E_1 bombard thin targets, and when bremsstrahlung from electrons of total energy E_1 bombard similar targets. In practice, it was convenient to measure the ratio of these yields by employing sanduiches, made up of two thin targets separated by a thin radiator, following the method described by Brown and Wilson[3].

The experimental ratio $R_{exp} = (Y_{br}/Y_e)$ was then compared with the ratio predicted by theory:

$$R_{th} = \frac{N_r \int_0^{E_1 - m_e} \sum_{\lambda L} \sigma_\gamma^\lambda (L,\omega)\ \phi\ (E_1,\omega,Z_r)\ \frac{d\omega}{\omega}}{\int_0^{E_1 - m_e} \sum_{\lambda L} \sigma_\gamma^\lambda (L,\omega)\ N^{(\lambda L)}(E_1,\omega)\ \frac{d\omega}{\omega}} \qquad (7)$$

where ϕ is the thin target bremsstrahlung intensity spectrum produced in the effective radiator of atomic number Z_r with N_r atoms/cm^2.

In order to obtain the experimental ratio, from the measured activities of both targets, they were subjected to corrections due to the finite thicknesses of the targets and radiator. Corrections were made for the energy degradation of the incident electrons, activity induced by bremsstrahlung in the targets and multiple scattering.

As mentioned in section I, the photodisintegration cross-section was originally assumed to be either entirely E1 or E2. A fraction of each one was then found in order to fit experimental data to the theoretical ratio evaluated in PW.

As usual, the ratios were presented in units of $(Z_r^2 r_e^2 N_r)$, r_e being the classical electron radius. In these units the ratios are called F and become independet of N_r.

The photo to electrodisintegration ratios considered here refer to a) one neutron emission from the following nuclei: ^{63}Cu, ^{64}Zn, ^{109}Ag and ^{181}Ta measured by Brown and Wilson[3],

^{63}Cu measured by Scott, Hanson and Kerst[4], and by Hines[5] ^{12}C measured by Barber[6]; ^{197}Au and ^{181}Ta measured by Barber and Wiedling [7]; b) two neutron emission from ^{197}Au and c) three neutron emission from ^{181}Ta, also measured by Barber and Wiedling[7].

For light and medium weight nuclei (up to ^{109}Ag) results lie close to the PW predictions of pure M1, but they can be equally well explained in the plane wave approach by assuming a mixture of from 88% to 95% E1 with 12% to 5% E2 intensity. Because of the theoretical explanations of the giant resonance in terms of electric dipole transitions; the latter explanation was preferred. For high Z, Barber and Wiedling concluded that the quadrupole intensity would have to be about equal to the E1 in the case of Ta and even higher for Au, for the one neutron emission reaction. For those reactions where *2n* and *3n* are emitted, the required E2 intensity would be about 75% and 100% respectively. The experimental data could also be fitted assuming an intensity of about 30% electric monopole plus 70% electric dipole. As the authors pointed out, although there is no direct experimental evidence ruling against strong electric monopole and quadrupole transitions in the giant resonance region of heavy nuclei, their existences is unlikely from theoretical considerations and they suggested that the theoretical calculations were in error, as it assumed plane waves for the initial and final electrons.

III-RESULTS OF DW ANALYSIS

We assumed σ_γ as being only due to E1 transitions (expression (6)). The theoretical ratios obtained using PW and DW together with experimental data referred in section II are shown in Figs. 1 to 8. The curves labelled PW and DW were evaluated from the expressions:

$$F_{PW}^{(E1)} = (N_r/Z_r^2\ r_e^2\ N_r)\ \frac{\int_0^{E_1-m_e} \sigma_\gamma(\omega)\ \phi(E_1,\omega,Z_r)\ \frac{d\omega}{\omega}}{\int_0^{E_1-m_e} \sigma_\gamma(\omega)\ N_{PW}^{E1}(E_1,\omega)\ \frac{d\omega}{\omega}} \qquad (8)$$

$$F_{DW}^{(E1)} = (N_r/Z_r^2\ r_e^2\ N_r)\ \frac{\int_0^{E_1-m_e} \sigma_\gamma(\omega)\ \phi\ (E_1,\omega,Z_r)\ \frac{d\omega}{\omega}}{\int_0^{E_1-m_e} \sigma_\gamma(\omega)\ N_{DW}^{E1}(E_1,\omega,Z_t)\ \frac{d\omega}{\omega}} \qquad (9)$$

where, N_{PW}^{E1} is given in expression (2), ϕ is the Schiff bremsstrahlung spectrum for intermediate screening[9], σ_γ is the measured photo disintegration cross-section[11-13] and N_{DW}^{E1} is given by an analytical expression[10] which fits the calculations of Gargaro and Onley[2] for $\lambda = E$ and $L = 1$:

$$N_{DW}^{El}(E_1,\omega,Z_t) = N_{PW}^{El}(E_1,\omega) + \omega\left[1.29\times10^{-5}\exp(1.245Z_t^{1/3} - .052E_1)\right] \times (E_2+m_e)/(E_1+m_e) \qquad (10)$$

where Z_t is the target atomic number.

We discuss bellow the results obtained for each of the nuclei considered in section II.

For ^{64}Zn and ^{109}Ag, Figs. 3 and 4, the curves PW and DW may be subjected to greater uncertainties than the remaining cases analysed, since they were computed using cross-sections unfolded from bremsstrahlung yields. There are few experimental points in both cases and they lie closer to the DW curves.

For ^{63}Cu, Fig. 2, the measurements of Brown and Wilson and Heines lie closer to the DW curve, in reasonable agreement with it. The crosses and full circles refer to the same raw data, measured by Scott et al., with different assumptions for the corrections. For the crosses, it was assumed that all electrons in the material loose energy uniformily and that the energy at any depth in the foil is just the initial energy reduced by the average total energy loss due to ionization and radiation. The full circles were obtained correcting the raw data for energy loss using an energy loss spectrum[4]. The statistical errors are of the size of the full circles or smaller, but errors introduced by the corrections are not evaluated. For the lower energy point the total correction amounted to about 40%. Taking into account the possible uncertain-

ties introduced by the corrections, the agreement between full circles and the F_{DW} curve may be considered good. These points cover the energy region where the giant resonance cross-section is concentrated. A comparison between full circles and crosses shows the importance of the corrections near threshold.

Figs. 1 and 5 to 8 refer to measurements by Barber[6] and Barber and Wiedling [7]. For these measurements, the corrections due to the electrons energy loss were carried out through a term:

$$\frac{\delta(N_1+N_2)}{\delta E_1} \times \frac{(\Delta_t + \Delta_r)}{2} \qquad (11)$$

where N_1 and N_2 are the measured activities of front and back foils, respectively, and $(\Delta_t + \Delta_r)$ is the average total energy loss, due to ionization and radiation, in the target plus radiator, at the electron bombarding energy E_1. We believe that the observed discrepancies between theory and experiment near threshold in these cases may come from the dificulty in evaluating the slope of the yield curve in this region and from the use of total average energy loss. Thus, we will only concern our discussion to points a few MeV above threshold.

For ^{12}C, Fig. 1, agreemen with F_{DW} is good, but the difference between F_{PW} and F_{DW} is small, as expected for low Z.

For the one neutron emission reaction in ^{181}Ta and ^{197}Au

Figs. 5 and 6, the experimental points agree with F_{DW} within experimental errors.

For ^{197}Au, $2n$ emission reaction and ^{181}Ta, $3n$ emission reaction, Figs. 7 and 8, only the high energy experimental points lie close to the F_{DW} curves.

CONCLUSIONS

The DW analysis of the available experimental ratios of foto to electrodisintegration, in the giant resonance region, suggests that the photoabsorption process can be undertood assuming E1 transitions only. While for low values of Z the PW and DW analysis leed to similar results, as expected, for high values of Z the DW analysis seems clearly in better agreement with the experimental points.

Previous claims of the need to involve E2 or other transitions can be traced to the invalidity of the PW analysis. They do not seem justified if DW analysis is used.

The disagreement between the analysis and data, near threshold, may be due to unreliable corrections for beam absorption and energy degradation.

The virtual foton spectra of Gargaro and Onley seem adequate to the analysis performed but better experimental data is needed to understand the situation near

the threshold.

ACKNOWLEDGMENTS

We thank Dr.W.C.Barber for useful discussions, Dr. D.S.Onley for useful discussions and a copy of a computer program and Dr. I.C.Nascimento for the results on some calculations with the above program.

the threshold.

ACKNOWLEDGMENTS

We thank Dr.W.C.Barber for useful discussions, Dr. D.S.Onley for useful discussions and a copy of a computer program and Dr. I.C.Nascimento for the results on some calculations with the above program.

REFERENCES

1) J.A.Thie, C.J.Mullin and E.Guth, Phys.Rev. 87(1952)962.

2) W.W.Gargaro and D.S.Onley, Phys.Rev. C4(1971) 1032.

3) K.L.Brown and R.W.Wilson, Phys.Rev. 93(1954)443.

4) M.B.Scott, A.O.Hanson and D.W.Kerst, Phys.Rev. 100(1956)209

5) R.L.Hines, Phys.Rev. 105(1957)1534.

6) W.C.Barber, Phys.Rev. 111(1958)1642.

7) W.C.Barber and T.Wiedling, Nucl.Phys. 18(1960)575.

8) F.W.Firk, Ann.Rev. of Nucl. Sc. 20(1970)39.

9) H.W.Koch and J.W.Motz, Rev. Mod.Phys. 31(1959)920.

10) E.Wolynec, I.C.Nascimento and D.S.Onley (to be published).

11) S.C.Fultz, J.T.Caldwell, B.L.Berman, R.L.Bramblett and R.R. Harvey, Phys.Rev. B162(1967) 1098.

12) S.C.Fultz, R.L.Bramblett, J.T.Caldwell and R.R.Harvey, Phys. Rev. B133(1964)1149.

13) L.Katz and A.G.W.Cameron, Can. J.Phys. 29(1951)518.

14) B.C.Diven and G.M.Almy, Phys.Rev. 80(1950)407.

15) R.Bergere, H.Beil and A.Veyssiere, Nucl.Phys. A121(1968)463.

16) A.Veyssiere, H.Beil, R.Bergere, P.Carlos and A.Leptretre, Nucl.Phys. A159(1970)561.

FIGURE CAPTIONS

Fig.1 - F_{PW}, F_{DW} and experimental ratios from ref. [6])

Fig.2 - F_{PW}, F_{DW} and experimental ratios from ref.[4]) (crosses and dots), from ref.[3])(triangles) and from ref.[5]) (squares). Crosses and dots refer to same raw data, but different criteria in applying corrections.

Fig.3 - F_{PW}, F_{DW} and experimental ratios from ref.[3])

Fig.4 - F_{PW}, F_{DW} and experimental ratios from ref.[3])

Fig.5 - F_{PW}, F_{DW} and experimental ratios from ref.[7]) (triangles) and ref.[3])(squares).

Fig.6 - F_{PW}, F_{DW} and experimental ratios from ref.[7])

Fig.7 - F_{PW}, F_{DW} and experimental ratios from ref.[7])

Fig.8 - F_{PW}, F_{DW} and experimental ratios from ref.[7]).

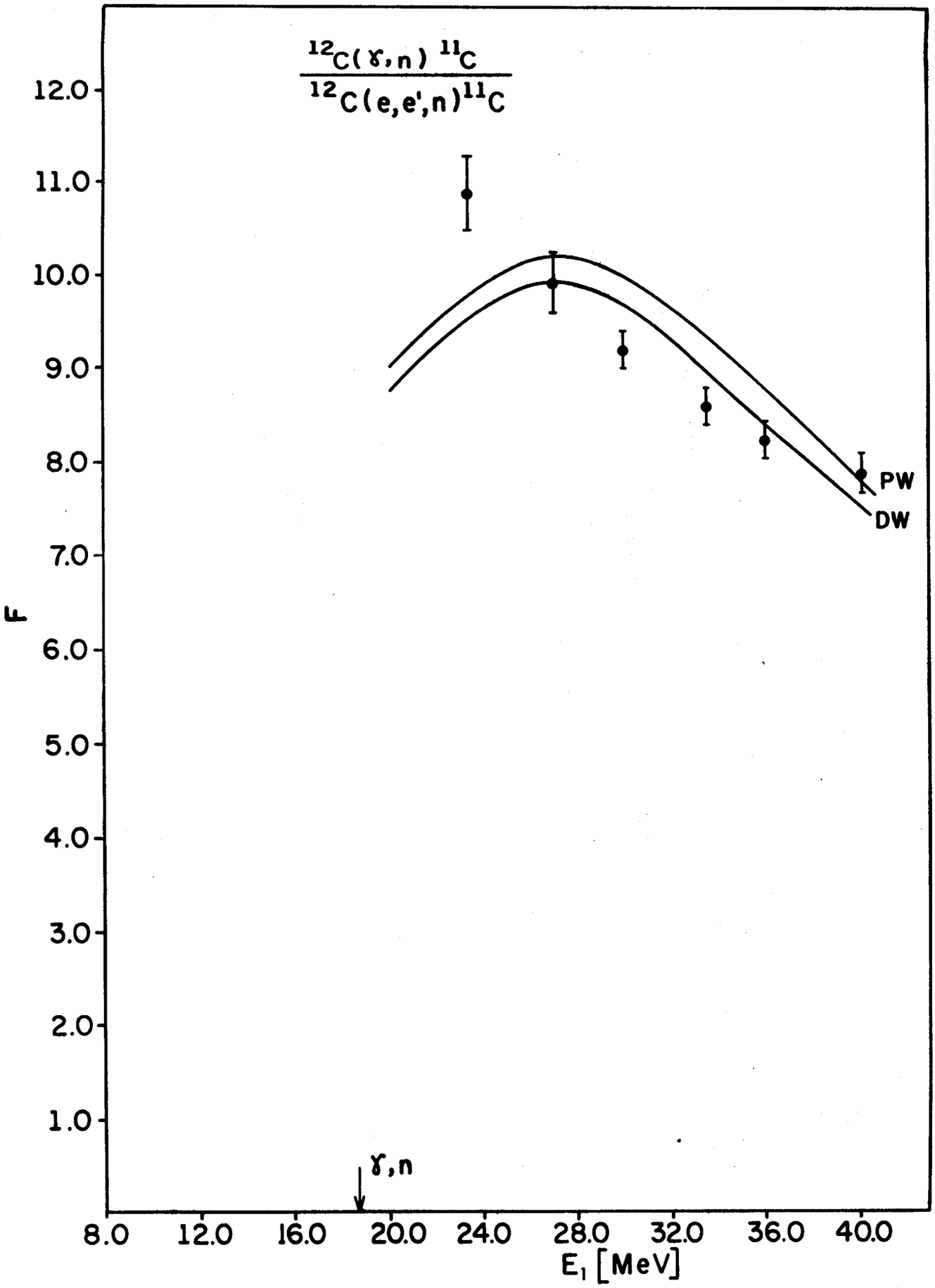
$\frac{^{12}C(\gamma,n)\,^{11}C}{^{12}C(e,e',n)^{11}C}$
12.0
11.0
10.0
9.0
8.0
7.0
6.0
5.0
4.0
3.0
2.0
1.0
F
PW
DW
γ,n
8.0
12.0
16.0
20.0
24.0
28.0
32.0
36.0
40.0
E_1 [MeV]

fig.1

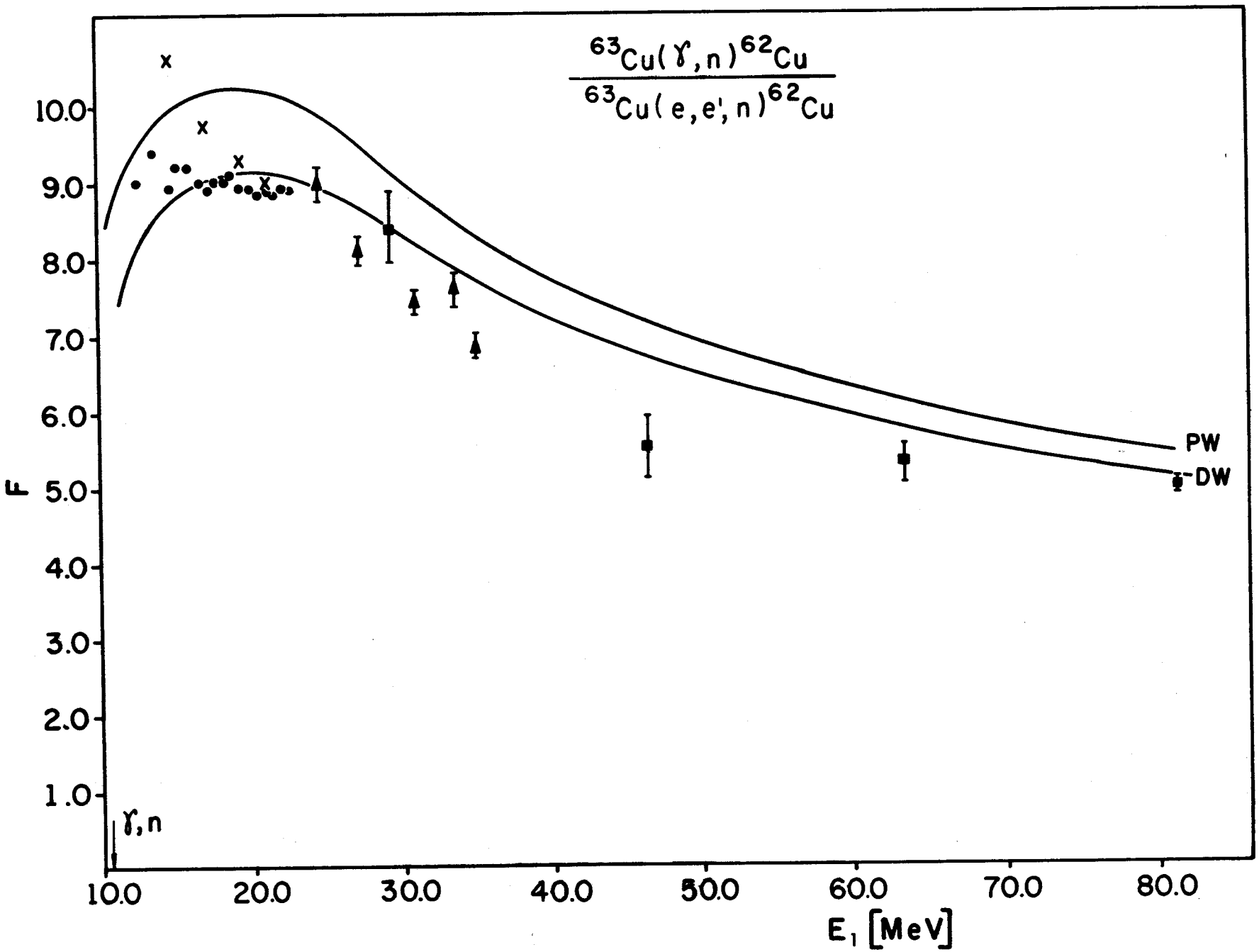
$^{63}Cu(\gamma,n)^{62}Cu$
$^{63}Cu(e,e',n)^{62}Cu$
F
10.0
9.0
8.0
7.0
6.0
5.0
4.0
3.0
2.0
1.0
PW
DW
γ,n
10.0
20.0
30.0
40.0
50.0
60.0
70.0
80.0
E_1 [MeV]

fig.2

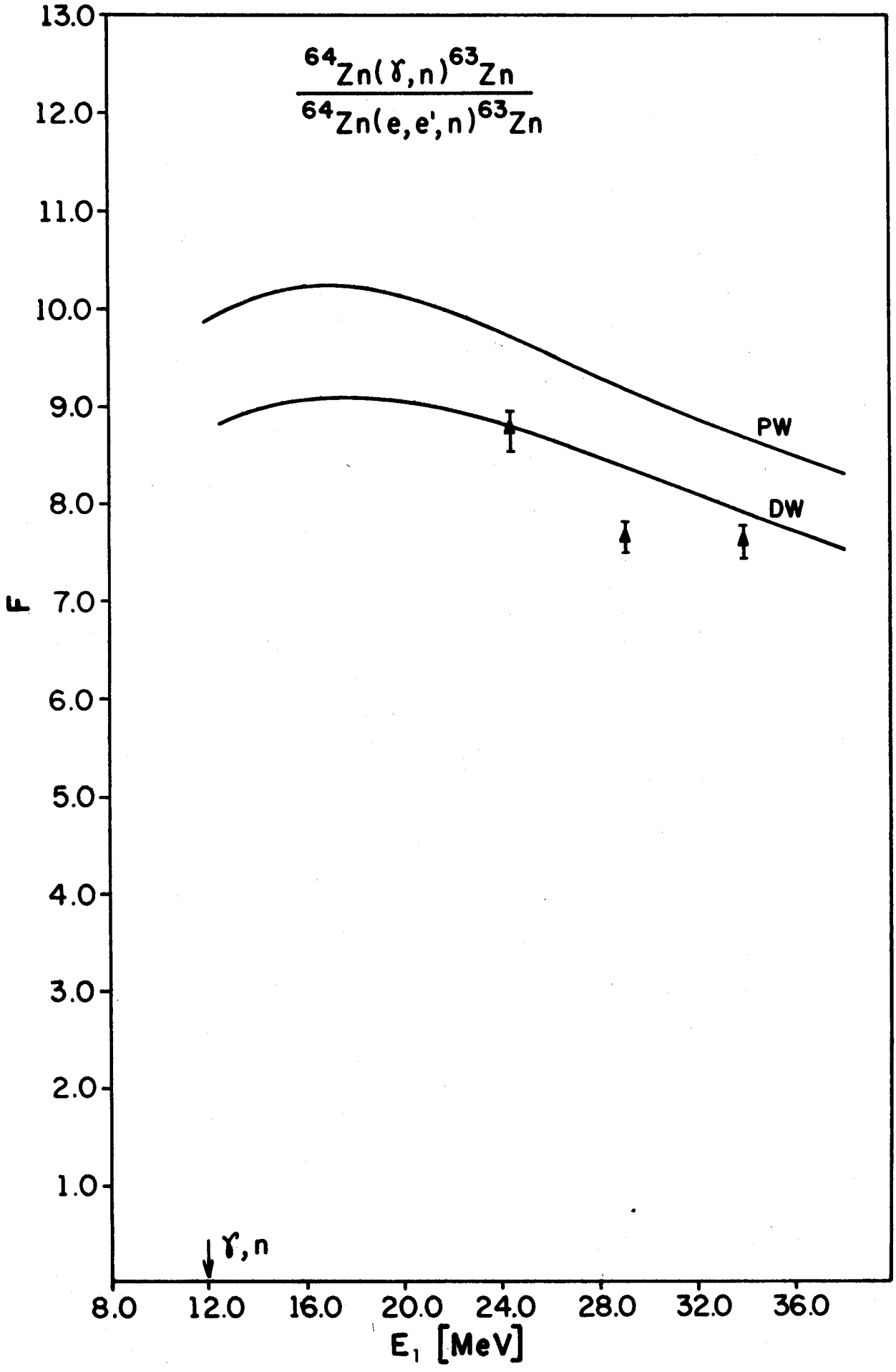
$^{64}Zn(\gamma,n)^{63}Zn$ / $^{64}Zn(e,e',n)^{63}Zn$
PW
DW
R
13.0
12.0
11.0
10.0
9.0
8.0
7.0
6.0
5.0
4.0
3.0
2.0
1.0
γ,n
8.0
12.0
16.0
20.0
24.0
28.0
32.0
36.0
E1 [MeV]

fig.3

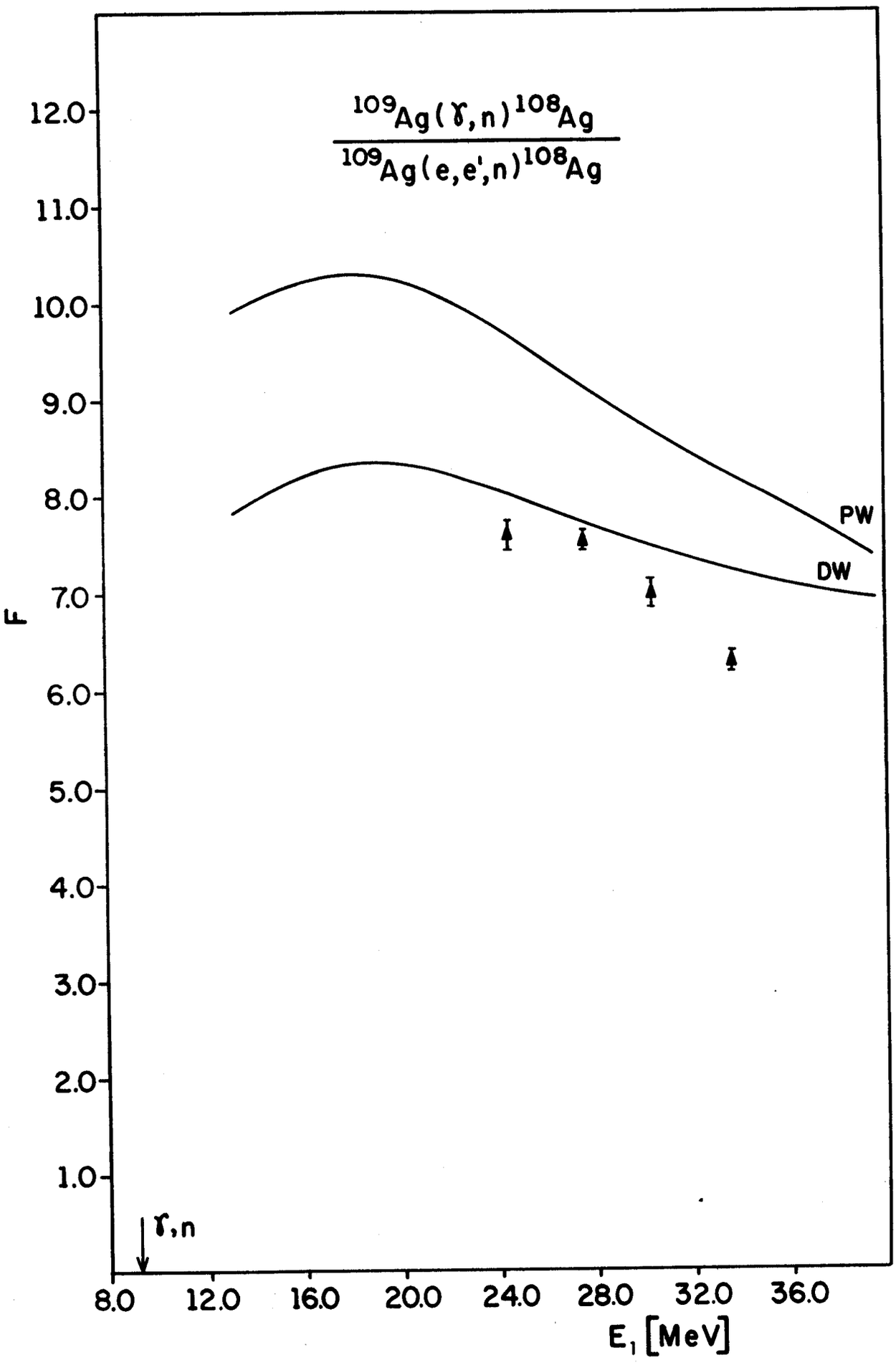
$^{109}Ag(\gamma,n)^{108}Ag$
$^{109}Ag(e,e',n)^{108}Ag$
12.0
11.0
10.0
9.0
8.0
7.0
6.0
5.0
4.0
3.0
2.0
1.0
F
PW
DW
γ,n
8.0
12.0
16.0
20.0
24.0
28.0
32.0
36.0
E_1 [MeV]

fig.4

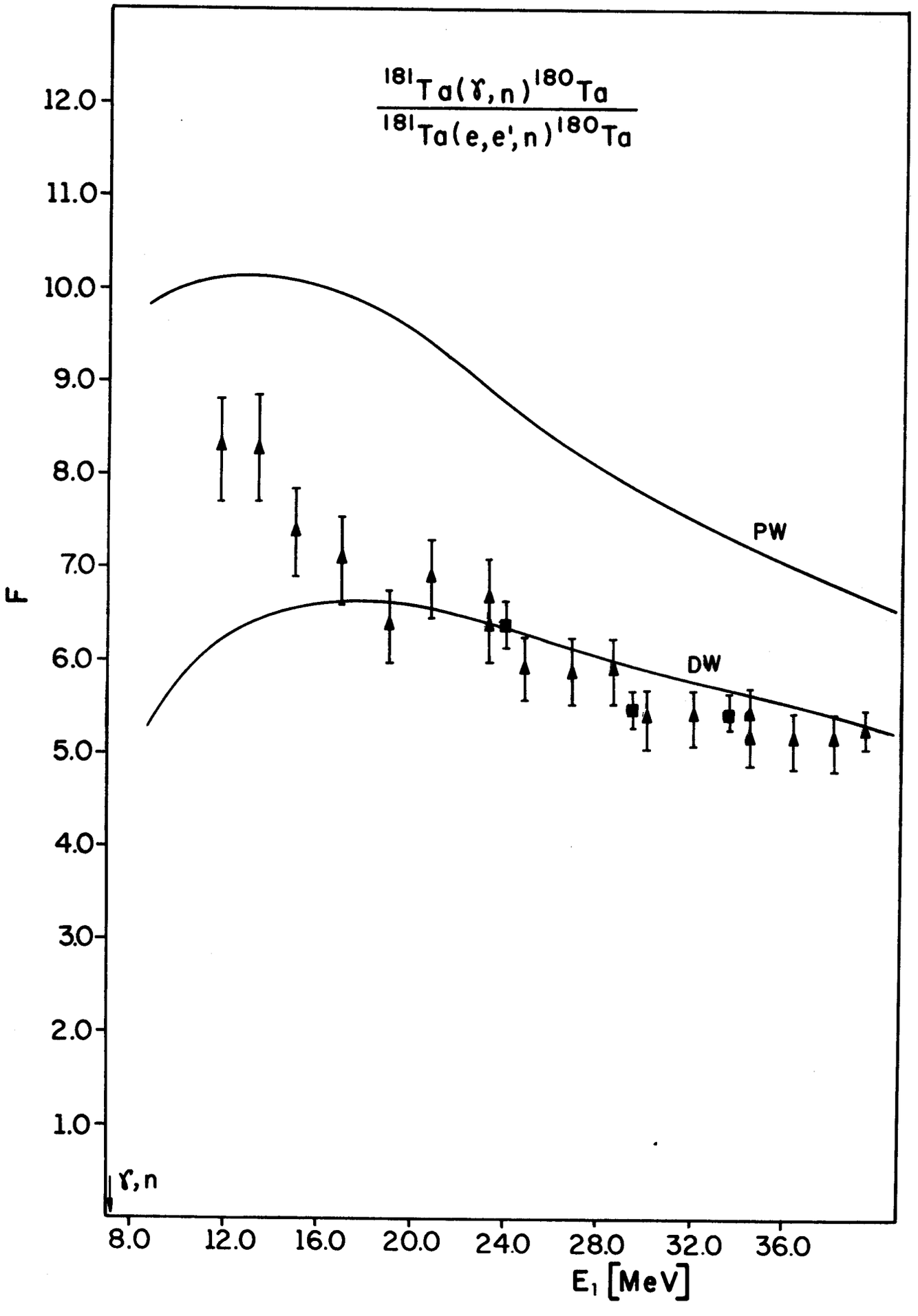
$^{181}Ta(\gamma,n)^{180}Ta$
$^{181}Ta(e,e',n)^{180}Ta$
PW
DW
F
12.0
11.0
10.0
9.0
8.0
7.0
6.0
5.0
4.0
3.0
2.0
1.0
γ,n
8.0
12.0
16.0
20.0
24.0
28.0
32.0
36.0
E_1 [MeV]

fig.5

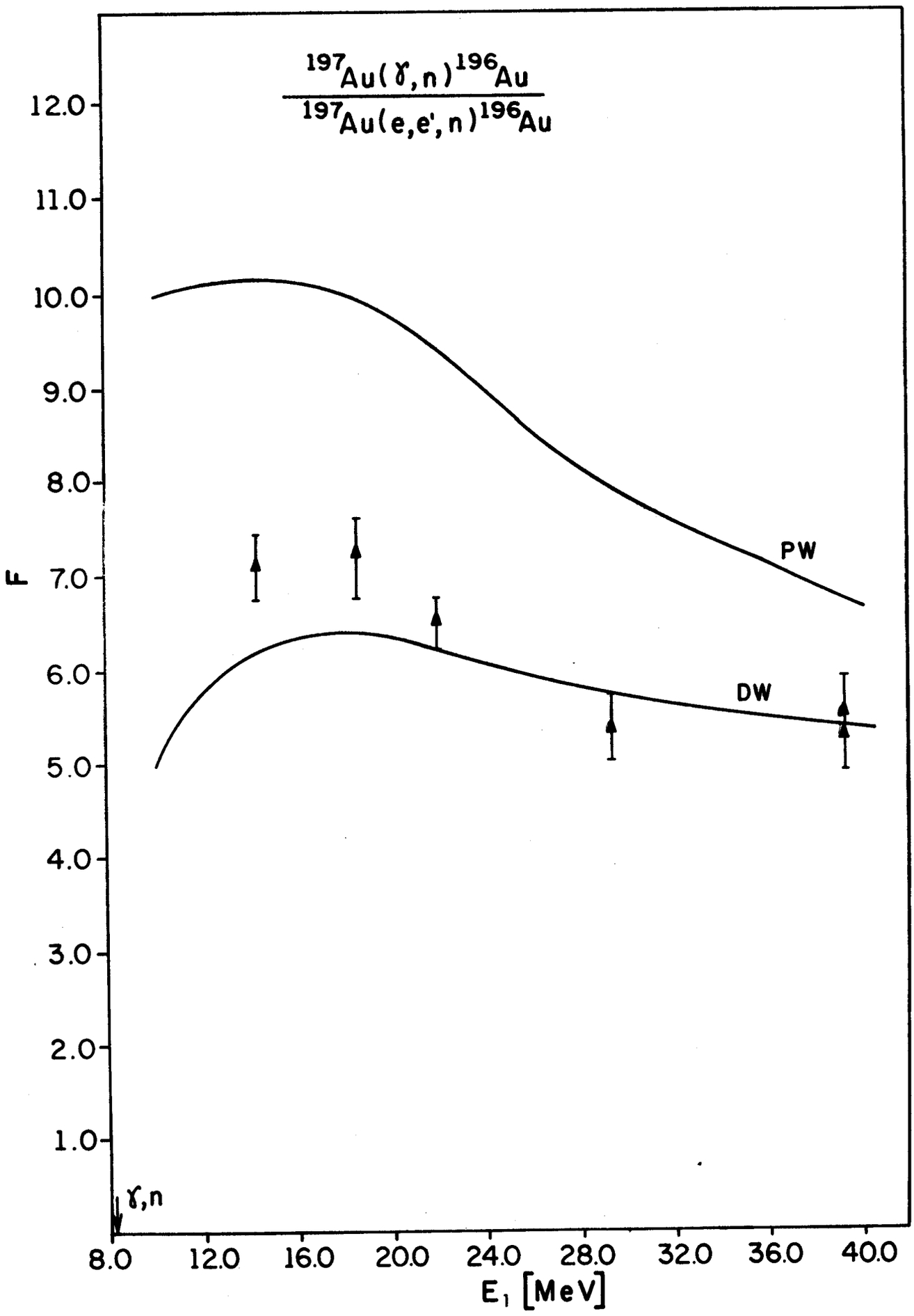
$\frac{^{197}Au(\gamma,n)^{196}Au}{^{197}Au(e,e',n)^{196}Au}$
12.0
11.0
10.0
9.0
8.0
7.0
6.0
5.0
4.0
3.0
2.0
1.0
F
PW
DW
γ,n
8.0
12.0
16.0
20.0
24.0
28.0
32.0
36.0
40.0
E₁ [MeV]

fig.6

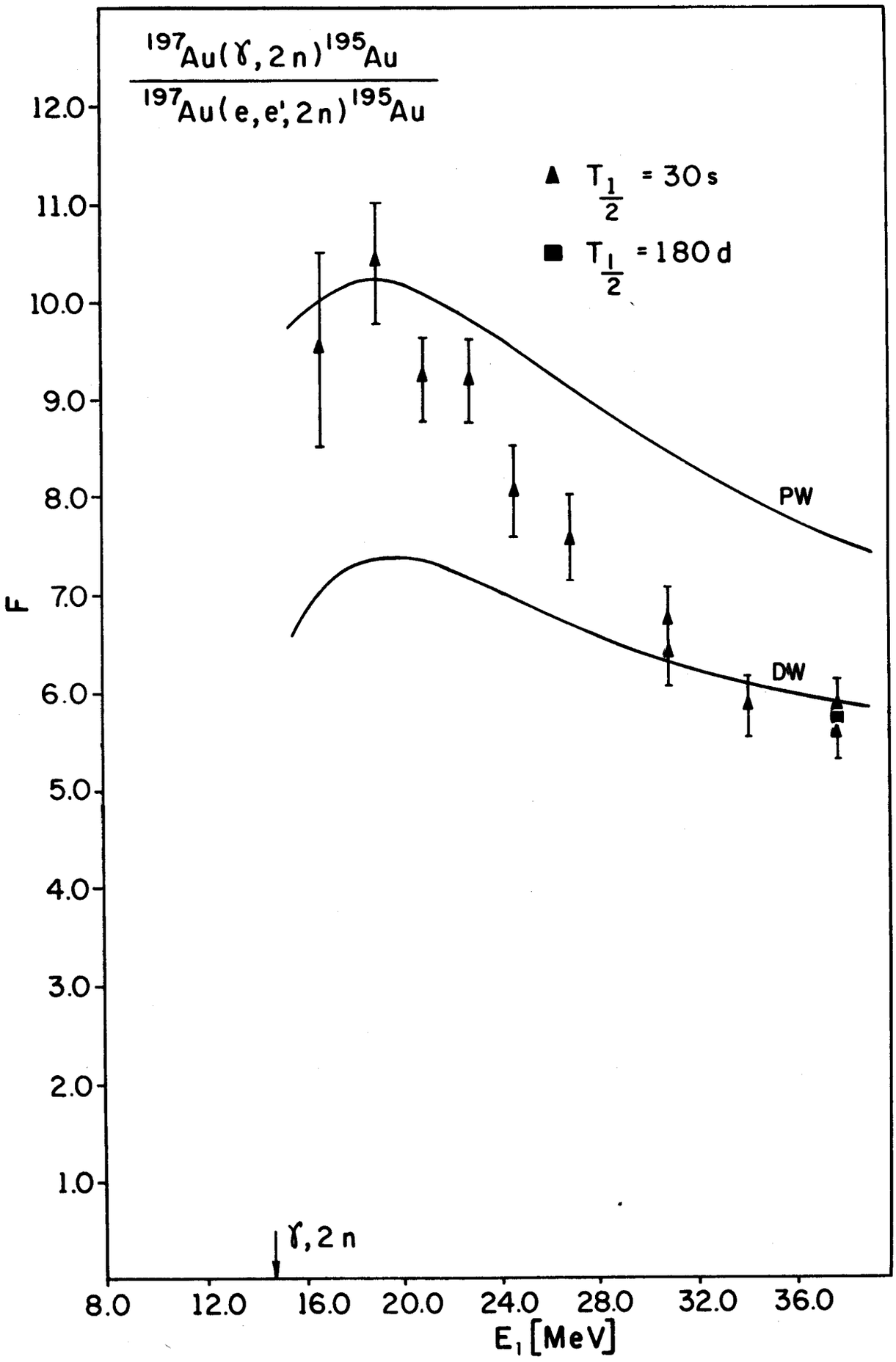
197Au(γ, 2n)195Au
197Au(e, e'; 2n)195Au
T1/2 = 30 s
T1/2 = 180 d
PW
DW
F
12.0
11.0
10.0
9.0
8.0
7.0
6.0
5.0
4.0
3.0
2.0
1.0
γ, 2n
8.0
12.0
16.0
20.0
24.0
28.0
32.0
36.0
E1 [MeV]

fig.7

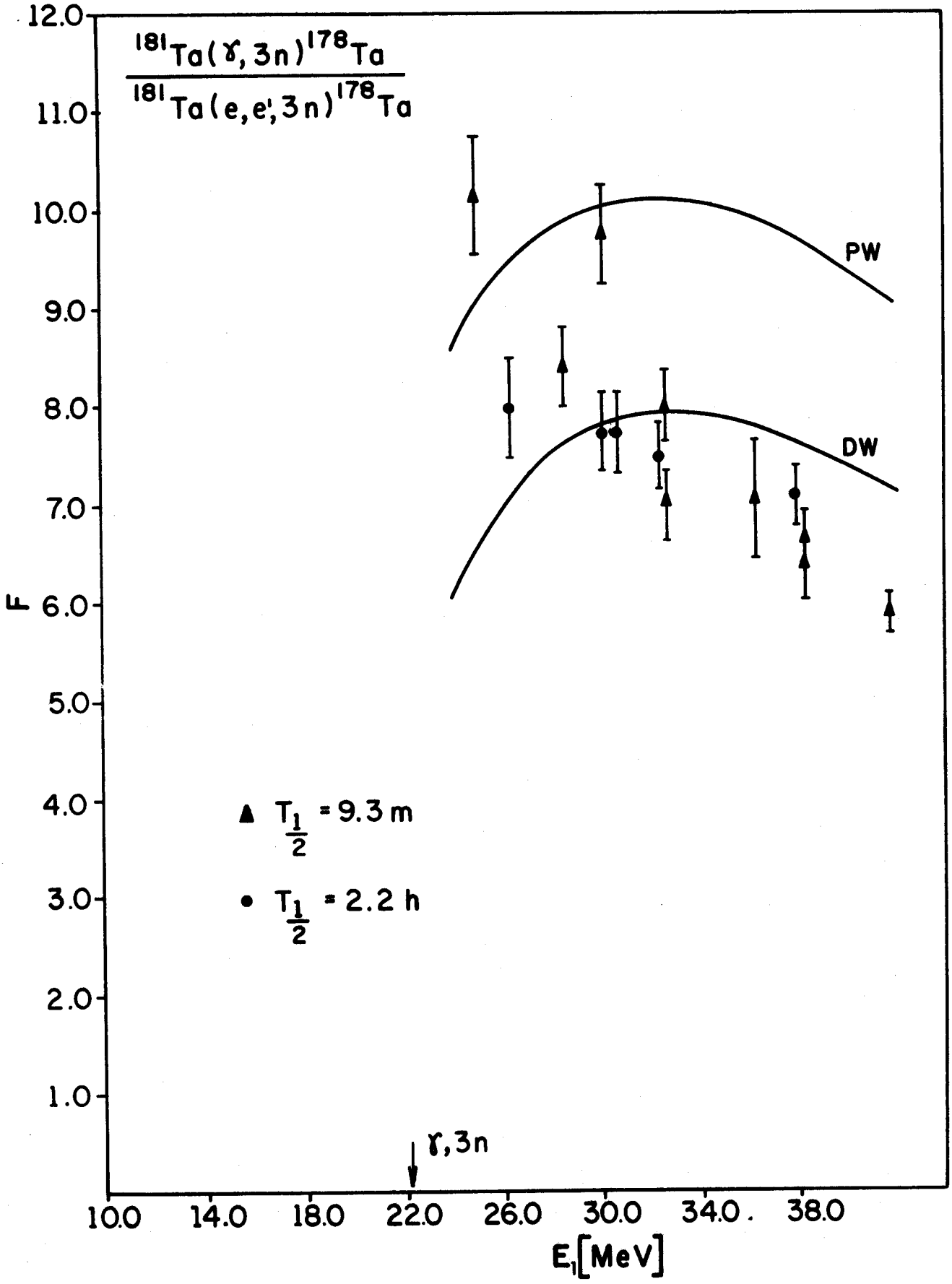
$^{181}Ta(\gamma, 3n)^{178}Ta$
$^{181}Ta(e, e', 3n)^{178}Ta$
PW
DW
▲ $T_{\frac{1}{2}}$ = 9.3 m
● $T_{\frac{1}{2}}$ = 2.2 h
F
γ, 3n
E_1[MeV]
12.0
11.0
10.0
9.0
8.0
7.0
6.0
5.0
4.0
3.0
2.0
1.0
10.0
14.0
18.0
22.0
26.0
30.0
34.0
38.0

fig.8